

# Spin eigen-excitations of the magnetic skyrmion and problem of the effective mass

Volodymyr P. Kravchuk,<sup>1,2,\*</sup> Denis D. Sheka,<sup>3</sup> Ulrich K. Röbler,<sup>2</sup> Jeroen van den Brink,<sup>2,4</sup> and Yuri Gaididei<sup>1</sup>

<sup>1</sup>*Bogolyubov Institute for Theoretical Physics of National Academy of Sciences of Ukraine, 03680 Kyiv, Ukraine*

<sup>2</sup>*Leibniz-Institut für Festkörper- und Werkstoffforschung, IFW Dresden, D-01171 Dresden, Germany*

<sup>3</sup>*Taras Shevchenko National University of Kyiv, 01601 Kyiv, Ukraine*

<sup>4</sup>*Institute for Theoretical Physics, TU Dresden, 01069 Dresden, Germany*

(Dated: October 12, 2018)

Properties of magnon modes localized on a ferromagnetic skyrmion are studied. Three types of possible asymptotic behavior of the modes eigenfrequencies are found for the case of large skyrmion radius  $R_s$ , namely  $\omega_0 \sim R_s^{-2}$  for the breathing mode,  $\omega_{-|\mu|} \sim R_s^{-1}$  and  $\omega_{|\mu|} \sim R_s^{-3}$  for modes with negative and positive azimuthal quantum numbers, respectively. A number of properties of the magnon eigenfunctions are determined. This enables us to demonstrate that the skyrmion dynamics based on the traveling wave model is described by the massless Thiele equation.

PACS numbers: 75.10.Hk, 75.10.Pq, 75.40.Mg, 75.60.Ch, 75.78.Cd, 75.78.Fg

## I. INTRODUCTION

Chiral magnetic skyrmion [1–8] are particle-like topological solitons with an integer topological charge (skyrmion number). In contrast to magnetic vortex [9–11], which has half-integer topological charge, skyrmion is a truly localized excitation. As a consequence, the dynamics of the skyrmion is insensitive to the size and shape of a sufficiently large sample, and remote skyrmions do not interact with each other, except the weak stray field effects. This is in strong contrast to magnetic vortices. The possibility to manipulate skyrmions as an “individual particles” together with the topological stability of this “particles” results in a large number of studies during the last years, where skyrmions are considered as key elements for nonvolatile memory and logic devices [3, 12–16]. This composed the new area of spintronics – skyrmionics [15].

On the other hand, magnon spintronics [17] is another recently emergent area of spintronics, which is intensively developing in parallel to the skyrmionics. Magnon transistor [18] and a number of the wave-based logic devices [17, 19] are proposed as key elements for the concept of the wave-based computing [17]. In this regard, the combination of these two trends (e.g. skyrmion-based nonvolatile memory and magnon-based logic devices) can give a significant push in the development of magnetic computer elements alternatively to the existed semiconductor chips. However, in this case, a deep understanding of properties of the skyrmion magnon modes is required.

The spectrum of linear excitations of any system reflects its fundamental properties, e.g. it enables one to find out conditions of instabilities and analyze their types. Knowledge of spectral dependencies opens wide opportunities for the resonance experimental techniques [20–22]. The presence of the skyrmion resonances can be considered as a proof of presence of skyrmions in the system and values of the eigenfrequencies can be used for determination of values of the material parameters.

Due to the fundamental interest and high importance for the applications the number of studies of magnon

spectra of skyrmions were recently carried out [23–32]. However, most of these studies are numerical and the existing theories are far from the completeness. Some important questions are still not clear, e.g. the presence of the high-frequency gyrotropic mode, which is a counterpart to the zero translational mode. It has the same azimuthal symmetry but nonzero eigenfrequency. In some models this mode is responsible for the formal appearance of mass of the topological soliton [10, 28, 29, 33–40], see discussion in Sec. V. In most of the mentioned studies this mode was not found [23–26]. On the other hand, it was found for some cases of large-radius skyrmions [28–30].

In this paper we present a detailed study and classification of the skyrmion magnon spectrum. The paper is build as follows. Section II is declaratory in nature, here we explain our model and introduce a system of the dimensional units used in the paper, see Table I. In Sec. III we consider the simplest case of the radially symmetrical magnon mode, so called breathing mode. The general study of the magnon spectrum is presented in Sec. IV. Here we obtain the asymptotic behavior of the eigenfrequencies of all localized modes. Additionally we find out a number of properties of the modes eigenfunctions, e.g. the orthogonality condition. These properties are utilized in Sec. V, where we use the collective variables approach in order to demonstrate that the skyrmion dynamics based on the traveling wave model is described by the *massless* Thiele equation.

## II. MODEL AND STATIC EQUILIBRIUM SOLUTIONS

Here we consider the case of chiral skyrmion, which is stabilized in perpendicular easy-axis ferromagnetic film without external magnetic field influence. The advantage of the field-free case is that the skyrmion can have an arbitrary large radius. However, the problem of the magnon spectrum is still not studied systematically for this case.

arXiv:1711.10461v1 [cond-mat.str-el] 28 Nov 2017

quantity	unit of measurement	value for Pt/Co/AlO <sub>x</sub> layer structure [41]
length	$\ell = \sqrt{A/K}$	5.6 nm
time	$\Omega_0^{-1} = \left(\frac{2K\gamma_0}{M_s}\right)^{-1}$	98 ps ( $\Omega_0 = 10.2$ GHz)
energy	$E_{\text{BP}} = 8\pi AL$	$4 \times 10^{-19}$ J (for $L = 1$ nm)
mass	$\mathcal{M}^* = L \frac{M_s^2}{K\gamma_0^2}$	$2.4 \times 10^{-21}$ kg (for $L = 1$ nm)
DMI strength	$\sigma = \sqrt{AK}$	2.9 mJ/m <sup>2</sup>

TABLE I. Units of physical quantities, which are used in this paper. Values are calculated for the following material parameters:  $A = 1.6 \times 10^{-11}$  J/m,  $M_s = 1.1 \times 10^6$  A/m and  $K = K_0 - 2\pi M_s^2 = 5.1 \times 10^5$  J/m<sup>3</sup> with  $K_0 = 1.3 \times 10^6$  J/m<sup>3</sup> being the intrinsic magneto-crystalline anisotropy.

In our model we take into account three contributions into the total energy of the ferromagnetic film

$$E = L \int [A\mathcal{E}_{\text{ex}} + K(1 - m_z^2) + D\mathcal{E}_{\text{D}}] dS, \quad (1)$$

here the integration is performed over the film area and  $L$  is the film thickness, which is assumed to be small enough to ensure uniformity of the magnetization in the perpendicular direction. The first term of the integrand is the exchange energy density with  $\mathcal{E}_{\text{ex}} = \sum_{i=x,y,z} (\partial_i \mathbf{m})^2$ , and  $A$  is the exchange constant. Here  $\mathbf{m} = \mathbf{M}/M_s$  is the unit magnetization vector with  $M_s$  being the saturation magnetization. The second term is the perpendicular easy-axis anisotropy with  $K > 0$  and  $m_z = \mathbf{m} \cdot \hat{\mathbf{z}}$  is the magnetization component normal to the surface. The last term represents the Dzyaloshinskii-Moriya interaction (DMI) with  $\mathcal{E}_{\text{D}} = m_z \nabla \cdot \mathbf{m} - \mathbf{m} \cdot \nabla m_z$ . This inhomogeneous DMI is associated with the  $C_{\infty v}$  symmetry of (idealized) ultrathin films [7, 42, 43] or bilayers [44], stems from the relativistic spin-orbit coupling [45, 46], and selects a fixed sense of rotation for any twisted noncollinear magnetization configuration.

In the following we introduce a system of dimensionless units, explained in the Table I. The proposed units of measurement have the following physical sense: magnetic length  $\ell$  is a typical width of a domain wall in the given system with vanishing DMI and  $\sigma$  is the energy per unit area of such a domain wall,  $\Omega_0$  is frequency of the uniform ferromagnetic resonance with  $\gamma_0$  being the gyromagnetic ratio,  $E_{\text{BP}}$  is energy of Belavin-Polyakov soliton [47], which coincides with energy of a skyrmion with infinitesimally small radius.

The constraint  $|\mathbf{m}| = 1$  is encoded by using the spherical angular parameterization  $\mathbf{m} = \sin \theta \cos \phi \hat{\mathbf{x}} + \sin \theta \sin \phi \hat{\mathbf{y}} + \cos \theta \hat{\mathbf{z}}$ . Magnetization dynamics is described by Landau-Lifshitz equations

$$\sin \theta \dot{\phi} = 4\pi \frac{\delta \mathcal{E}}{\delta \theta}, \quad \sin \theta \dot{\theta} = -4\pi \frac{\delta \mathcal{E}}{\delta \phi}, \quad (2)$$

where the overdot denotes the derivative with respect to the dimensionless time  $\tau = t\Omega_0$ , and  $\mathcal{E} = E/E_{\text{BP}}$  is the dimensionless energy. Here and below, all distances are measured in units  $\ell$ , in accordance with Table I.

For the proposed system of units the dimensionless DMI constant  $d = D/\sigma$  is the only parameter, which controls the system. The described model is characterized by the critical value of the DMI constant  $d_0 = 4/\pi$ , which separates two ground states, namely the uniform state  $\mathbf{m} = \pm \hat{\mathbf{z}}$  for the case  $|d| < d_0$ , and helical periodical state for  $|d| > d_0$  [6, 41, 46, 48–50]. For the case  $0 < |d| < d_0$  Eqs. (2) have a stationary skyrmion solution  $\theta = \Theta(\rho)$  and  $\phi = \Phi(\chi)$ , where  $\Phi = \chi + \Psi_0$  and  $\{\rho, \chi\}$  are polar coordinates. This is an excitation of the uniform ground state. The skyrmion profile is determined by equation [5, 6, 41, 49, 50]

$$\begin{aligned} \Delta_\rho \Theta - \sin \Theta \cos \Theta \left(1 + \frac{1}{\rho^2}\right) + \frac{|d|}{\rho} \sin^2 \Theta &= 0, \\ \Theta(0) = \pi, \quad \Theta(\infty) &= 0. \end{aligned} \quad (3)$$

where  $\Delta_\rho f = \rho^{-1} \partial_\rho (\rho \partial_\rho f)$  is radial part of the Laplace operator. For the case of boundary conditions (3) one has  $\Psi_0 = 0$  if  $d > 0$ , and  $\Psi_0 = \pi$  if  $d < 0$ . In the other words, the considered type of DMI induces so called Néel (hedgehog) skyrmion. The case of an alternative boundary conditions  $\Theta(0) = 0$  and  $\Theta(\infty) = \pi$  is not considered here, because it does not result in fundamentally new properties of the magnon spectra compared to (3).

### III. LARGE-RADIUS SKYRMION AND RADIALLY SYMMETRICAL MODE

The skyrmion profile is a localized function [6, 41, 49, 50], this enables one to introduce the skyrmion radius  $R_s$  as solution of the equation  $\cos \Theta(R_s) = 0$ . Skyrmion radius  $R_s$  strongly depends on the DMI constant [6, 41]:  $R_s \rightarrow 0$  when  $d \rightarrow 0$  (skyrmion collapse), while  $R_s \rightarrow \infty$  when  $d \rightarrow \pm d_0$ , see Fig. 1(a). For a large-radius skyrmion  $R_s \gg 1$  one can easily estimate the asymptotic behavior of  $R_s$ . In this case the skyrmion profile is well described by the circular domain wall Ansatz

$$\cos \theta = \tanh \frac{\rho - R_s}{\Delta}, \quad \phi = \chi + \Psi \quad (4)$$

Here the skyrmion radius  $R_s$ , phase  $\Psi$  and width  $\Delta$  are treated as collective variables. This is in contrast to the number of the previous papers [28, 37, 41], where the model (4) was used for the constant  $\Delta$ . Normalized energy of the skyrmion, which is described by the model (4), reads

$$\mathcal{E} \approx \frac{1}{2} \left( \underbrace{\frac{R_s}{\Delta} + \frac{\Delta}{R_s}}_{\text{exchange}} - \underbrace{2\delta R_s \cos \Psi}_{\text{DMI}} + \underbrace{\Delta R_s}_{\text{anisotr.}} \right), \quad (5)$$

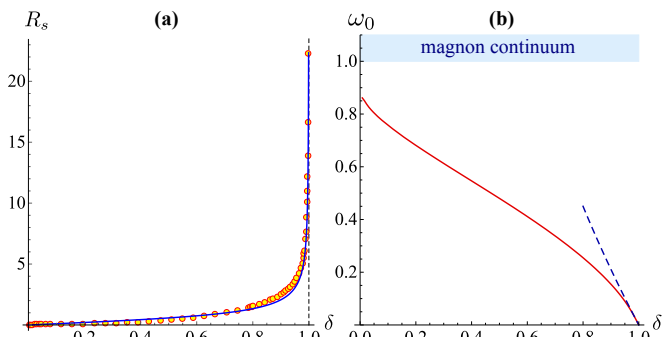


FIG. 1. (a) Skyrmion radius as a function of the normalized DMI constant. Line shows the estimation (6) while dots correspond to the exact numerical solutions of Eq. (3). (b) Breathing mode eigenfrequency (solid line) and asymptotics (9) (dashed line) for the case of large skyrmion radius ( $\delta \gtrsim 1$ ).

where  $\delta = d/d_0$  is normalized DMI constant. Minimum of the energy (5) is reached for the following equilibrium values of the collective variables:  $\Delta_0 = |\delta|$  and  $\Psi_0 = 0$  ( $\Psi_0 = \pi$ ) when  $\delta > 0$  ( $\delta < 0$ ). And the skyrmion radius reads

$$R_s \approx |\delta|/\sqrt{1 - \delta^2}. \quad (6)$$

In the limit case  $\delta \rightarrow 1$  the estimation (6) is transformed to the previously proposed one [41]  $R_s \approx 1/\sqrt{2(1 - \delta)}$ , which was obtained for the constant width  $\Delta = 1$ . The obtained estimation agrees well with the exact values of  $R_s$  for the all range of the DMI constant, not only for the case  $R_s \gg 1$ , see Fig. 1(a).

Let us now consider excitation of the radially symmetrical mode. This can be easily done by considering the time dependent dynamics of the collective variables  $R_s(t)$  and  $\Psi(t)$  in vicinity of their equilibrium values. To this end we treat the equations of motion (2) as extrema of the action functional  $S = \int \mathcal{L} d\tau$  with the Lagrange function

$$\mathcal{L} = \frac{1}{4\pi} \int (1 - \cos \theta) \dot{\phi} dS - \mathcal{E}. \quad (7)$$

Ansatz (4) represents a circularly closed domain wall. It is well known [51–55] that dynamics of the width  $\Delta$  of the 1D domain wall has essentially different timescale as compared to the timescale of the domain wall position ( $R_s$ ) and phase ( $\Psi$ ), namely  $\Delta$  fast relaxes towards its equilibrium value determined by the much slower variables  $R_s$  and  $\Psi$ . Therefore, an assumption that  $\Delta$  is a “slave” variable works very well in the most cases. Here we assume that the same is true for the circularly closed domain wall if  $R_s \gg 1$ . In this case the substitution of Ansatz (4) into (7) results in the following effective Lagrange function

$$\begin{aligned} \mathcal{L}^{\text{eff}} &= \dot{\Psi} R_s^2 - \mathcal{E}^{\text{eff}}, \\ \mathcal{E}^{\text{eff}} &= R_s \left( \frac{1}{|\delta|} - 2\delta \cos \Psi + |\delta| \right) + \frac{|\delta|}{R_s}. \end{aligned} \quad (8)$$

As follows from (8) the skyrmion area is the canonically conjugated momentum for the skyrmion phase. The effective Lagrange function (8) generates a set of two equations of motion for  $\Psi$  and  $R_s$ , which have a static equilibrium solutions (6) and  $\Psi_0$ , which is determined above. The corresponding linear dynamics in vicinity of the equilibrium state is characterized by the eigenfrequency

$$\tilde{\omega}_0 = \frac{1 - \delta^2}{|\delta|} = \frac{1}{R_s \sqrt{1 + R_s^2}} \approx \frac{1}{R_s^2}. \quad (9)$$

The corresponding asymptotics are shown in Fig. 1(b) and Fig. 2(b).

#### IV. GENERAL DESCRIPTION OF THE MAGNON SPECTRA

The dispersion relation of linear excitations (magnons) of the uniform ground state is not influenced by the DMI and coincides with the common dispersion for the easy-axis magnets  $\omega = 1 + q^2$  with  $q = kl$  being the dimensionless wave-number. Thus, one has the continuum spectrum with  $\omega \geq 1$  for the frequencies above the anisotropy-induced gap. In the following we are interested in magnons over the equilibrium skyrmion state. For this purpose we introduce small excitations of the stationary solution:  $\theta = \Theta + \vartheta$ ,  $\phi = \Phi + \varphi/\sin \Theta$ . Equations (2) linearized with respect to the excitations results in

$$\begin{cases} \dot{\varphi} = -\Delta \vartheta + U_1 \vartheta + W \partial_\chi \varphi, \\ -\dot{\vartheta} = -\Delta \varphi + U_2 \varphi - W \partial_\chi \vartheta. \end{cases} \quad (10a)$$

Here the Laplace operator has the form  $\Delta = \Delta_\rho + \rho^{-2} \partial_{\chi\chi}^2$  and the potentials are as follows

$$\begin{aligned} U_1 &= \cos 2\Theta \left( 1 + \frac{1}{\rho^2} \right) - \frac{|d|}{\rho} \sin 2\Theta, \\ U_2 &= \cos^2 \Theta \left( 1 + \frac{1}{\rho^2} \right) - \Theta'^2 - |d| \left( \Theta' + \frac{\sin \Theta \cos \Theta}{\rho} \right), \\ W &= \frac{2}{\rho^2} \cos \Theta - \frac{|d|}{\rho} \sin \Theta. \end{aligned} \quad (10b)$$

Here a prime denotes derivative with respect to  $\rho$ . Equations (10) have a solution  $\vartheta(\rho, \chi, \tau) = f(\rho) \cos(\omega\tau + \mu\chi + \eta)$ ,  $\varphi(\rho, \chi, \tau) = g(\rho) \sin(\omega\tau + \mu\chi + \eta)$ , where the azimuthal wave number  $\mu \in \mathbb{Z}$  determines the nodes number ( $2|\mu|$ ) when moving around the skyrmion center in azimuthal direction, and  $\eta$  is an arbitrary phase. The eigenfrequencies  $\omega$  and the corresponding eigenfunctions  $f, g$  are determined by the following eigenvalue problem (EVP)

$$H\psi = \omega \sigma_x \psi. \quad (11a)$$

for a Hermitian operator

$$H = \begin{pmatrix} -\Delta_\rho + \frac{\mu^2}{\rho^2} + U_1 & \mu W \\ \mu W & -\Delta_\rho + \frac{\mu^2}{\rho^2} + U_2 \end{pmatrix}. \quad (11b)$$

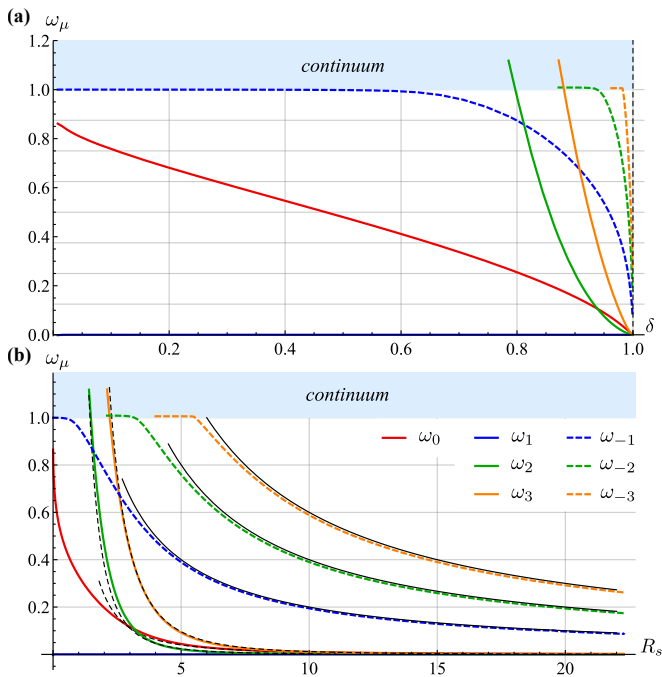


FIG. 2. The eigenfrequencies  $\omega_\mu$  of localized modes as functions of the normalized DMI constant  $\delta = d/d_0$  (a) and skyrmion radius (b) are obtained by means of numerical solution of the EVP (11). Thin lines are the asymptotes (13) for the case  $R_s \gg 1$ . Modes with  $|\mu| > 3$  are not shown. Frequency  $\omega_1$  belongs to the zero translational mode, while  $\omega_{-1}$  corresponds to the high-frequency gyrotropic mode.

Here  $\psi = (f, g)^T$ , and  $\sigma_x$  is the first Pauli matrix. The formulated EVP (11) structurally coincides with the corresponding EVP previously formulated for the case of magnons over precessional solitons in easy-axis magnets [37–39], magnetic vortices in easy-plane magnets [36, 56], and magnetic skyrmions [23–26]. Note that there is an alternative formulation of (10) in form of the generalized Schrödinger equation [38, 56], see Appendix B for details.

The EVP (11) is analyzed both analytically and numerically, for details see Appendix A. Equations (11) are invariant with respect to the simultaneous change of sign of three quantities:  $\omega \rightarrow -\omega$ ,  $\mu \rightarrow -\mu$  and  $f \rightarrow -f$  (or  $g \rightarrow -g$ ). This invariance results in a symmetry of the spectrum, which simplifies classification of the modes: one can fix either sign of  $\mu$  considering both signs of  $\omega$  or one can fix sign of  $\omega$  considering both signs of  $\mu$ . Following the previous studies [23, 36–38, 56] we choose the latter classification and consider nonnegative frequencies  $\omega \geq 0$ .

A number of localized modes are found below the edge of the continuum spectrum. Frequencies of the localized modes strongly depend on the DMI constant, see Fig. 2(a); alternatively we demonstrate the dependence on skyrmion radius, Fig. 2(b), which can be useful for applications. For any value of the skyrmion radius (DMI constant) there are at least three localized modes: radially symmetrical (breathing) mode  $|\mu = 0$  and two

modes  $|\pm 1\rangle$  which are called gyrotropic [40]. Due to the translational invariance one of the gyrotropic modes has zero eigenfrequency  $\omega_1 = 0$  (in our case this is the mode  $|+1\rangle$ ). This mode is called translational, it has the following eigenfunctions [57]  $f_1 = -\Theta'$  and  $g_1 = \sin \Theta/\rho$ , see Fig. 3. Although the other gyrotropic mode  $|-1\rangle$ , has the same azimuthal symmetry as the translational one, its eigenfunctions  $f_{-1}$  and  $g_{-1}$  are completely different, see Fig. 3. For a small radius skyrmion the eigenfrequency  $\omega_{-1}$  of the mode  $|-1\rangle$  practically coincides with the edge of the continuum, while for large skyrmions it is inversely proportional to the skyrmion radius, see Fig. 2(b). It is naturally to call the mode  $|-1\rangle$  high-frequency gyrotropic mode.

With the skyrmion radius increasing, the localized modes with higher azimuthal numbers  $|\mu| \geq 2$  appear in the gap. However, it is important to note that for a given  $\mu$  there is no more than one localized mode. Some examples of eigenfunctions of other localized modes are shown in Fig. 3. Far from the skyrmion the functions  $f_\mu$  and  $g_\mu$  have the same asymptotic behavior because  $U_1 \rightarrow U_2$  when  $\rho \rightarrow \infty$ . Note also that the localization area of the eigenfunctions increases when the corresponding eigenfrequency reaches the bottom of the continuum.

The eigenfunctions  $f_\mu$  and  $g_\mu$  has a number of properties, which are important for the future analysis. Here we present the orthogonality condition

$$\int_0^\infty \rho [f_\mu g_{-\mu} - f_{-\mu} g_\mu] d\rho = 0 \quad (12)$$

which follows from (A3) when the symmetry between branches  $\mu$  and  $-\mu$  is taken into account, for details see Appendix A. The analogous orthogonality condition was previously obtained for magnons over precessional solitons [39]. The other properties are listed in (A5), (A6), (A8), and (A11).

The found properties of the eigenfunctions enable us to find the eigenfrequencies asymptotics for the case of a large-radius skyrmion with  $R_s \gg 1$ :

$$\omega_0 \approx \frac{1}{R_s^2}, \quad \omega_\mu \approx \begin{cases} 2|\mu|/R_s, & \mu < 0, \\ c_\mu/R_s^3, & \mu > 0, \end{cases} \quad (13)$$

where  $c_\mu$  is a constant, for details see Appendix A. Comparison with the numerical solution enables one to suppose that  $c_\mu = \mu(\mu^2 - 1)/2$ . The asymptotics (13) are shown in Fig. 2 by the thin lines.

For the case  $|\delta| \rightarrow 1$  (or equivalently  $R_s \rightarrow \infty$ ) the number of local modes grows infinitely. And in the critical point  $|\delta| = 1$  all the modes become unstable (the frequencies of these modes vanish).

## V. EFFECTIVE MASS IN A COLLECTIVE VARIABLES APPROACH

Since the skyrmion is an exponentially localized excitation, there is an notion that its dynamics can be ap-

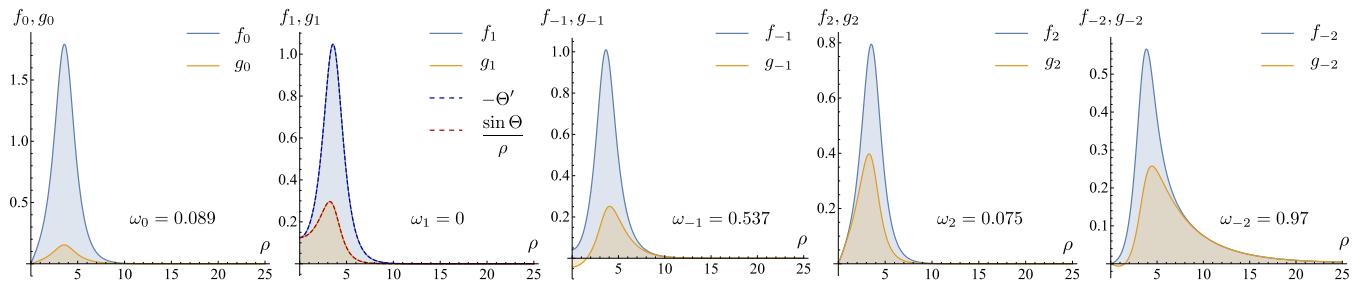


FIG. 3. Eigenfunctions and eigenfrequencies obtained by means of numerical solution of (11) for the case  $\delta = 0.95$  ( $R_s = 3.51$ ) and free boundary conditions. The eigenfunctions are normalized by the rule  $\alpha_\mu = 2$ .

proximated by dynamics of a point particle with coordinates  $\mathcal{R} = \{\mathcal{X}, \mathcal{Y}\}$ , which are called collective coordinates. However, the way of definition of the skyrmion center  $\mathcal{R}$  is not unique. For the first time, the essential dependence of the collective coordinates dynamics on the definition of  $\mathcal{R}$  was indicated in Ref. 39 for example of the precessional solitons. The recent analysis of numerically simulated skyrmion motion shows [49] that the different definitions result in essentially different types of trajectories  $\mathcal{R}(\tau)$ . In order to describe more complicated trajectories the internal degrees of freedom of skyrmion are involved into the consideration [28], which results in appearance of an effective mass term in the equations of motion for the collective coordinates [28, 40]. The aim of this section is to utilize the properties of the magnon eigenfunctions in order to (i) determine the physically sound definition of the skyrmion center; (ii) clarify the appearance of the effective mass term.

Collective variable approaches [58] are widely used for analysis of dynamics of soliton-like excitations in magnetic media [10, 55, 59–61]. They are based on the assumption that the time dependence of the continuum magnetization vector field  $\mathbf{m}$  can be reduced to the time dependence of a discrete set of collective variables  $\boldsymbol{\xi} = \{\xi_1, \xi_2, \dots\}$ , i.e.  $\mathbf{m}(\mathbf{r}, \tau) = \mathbf{m}(\mathbf{r}, \boldsymbol{\xi}(\tau))$ . This enables one to proceed from the couple of the partial differential equations (2) to the set of the ordinary differential equations (ODE)

$$\sum_j G_{\xi_i \xi_j} \dot{\xi}_j = \frac{\partial \mathcal{E}}{\partial \xi_i}, \quad (14)$$

$$G_{\xi_i \xi_j} = \frac{1}{4\pi} \int \sin \theta \left( \frac{\partial \theta}{\partial \xi_i} \frac{\partial \phi}{\partial \xi_j} - \frac{\partial \theta}{\partial \xi_j} \frac{\partial \phi}{\partial \xi_i} \right) dS,$$

where  $dS = dS/\ell^2$  is dimensionless area element. See also the tutorial papers Ref. 10 and 51.

A case where the only variables are collective coordinates describing placement of a soliton ( $\boldsymbol{\xi} = \mathcal{R}$ ) is called the traveling wave model  $\mathbf{m}(\mathbf{r}, \tau) = \mathbf{m}_0(\mathbf{r} - \mathcal{R}(\tau))$ , where  $\mathbf{m}_0$  is a stationary solution. Let us consider a more gen-

eral ansatz

$$\begin{aligned} \theta^{\text{an}}(\rho, \chi, \tau) &= \Theta(\rho) \\ &+ \sum_{\mu=-\infty}^{\infty} f_\mu(\rho) [\mathcal{A}_\mu(\tau) \cos \mu\chi + \mathcal{B}_\mu(\tau) \sin \mu\chi], \\ \phi^{\text{an}}(\rho, \chi, \tau) &= \chi + \Psi_0 \\ &+ \frac{1}{\sin \Theta(\rho)} \sum_{\mu=-\infty}^{\infty} g_\mu(\rho) [\mathcal{A}_\mu(\tau) \sin \mu\chi - \mathcal{B}_\mu(\tau) \cos \mu\chi], \end{aligned} \quad (15)$$

which corresponds to (A4) but only localized modes are taken into account. Here  $\Theta(\rho)$  determines the static skyrmion profile. The time-dependent collective variables  $\mathcal{A}_\mu, \mathcal{B}_\mu$  play the role of amplitudes of the magnon modes. Thus, in our case  $\boldsymbol{\xi} = \{\mathcal{A}_k, \mathcal{B}_k\}$  with  $k \in \mathbb{Z}$ .

First of all, it is important to note that the ansatz (15) includes the infinitesimal skyrmion displacements in sense of the traveling wave model. Indeed, the expansion of expressions

$$\begin{aligned} \theta &= \Theta \left( \sqrt{(x - \mathcal{X})^2 + (y - \mathcal{Y})^2} \right), \\ \phi &= \arctan \frac{y - \mathcal{Y}}{x - \mathcal{X}} + \Psi_0 \end{aligned} \quad (16)$$

in  $\mathcal{X}, \mathcal{Y}$  up to the linear terms and comparison with (15) results in

$$\mathcal{X} = \mathcal{A}_1, \quad \mathcal{Y} = \mathcal{B}_1, \quad (17)$$

if the form of the eigenfunctions  $f_1 = -\Theta'(\rho)$  and  $g_1 = \sin \Theta(\rho)/\rho$  is taken into account.

The second important observation is that the collective coordinates, which correspond to the traveling wave model, coincide with the first moment (center of mass) of the topological density:

$$\mathcal{R} = \frac{1}{4\pi\mathcal{Q}} \int \mathbf{r} \mathcal{J} dS, \quad (18)$$

where  $\mathcal{J} = -\mathbf{m} \cdot [\partial_x \mathbf{m} \times \partial_y \mathbf{m}]$  is the topological charge density and  $\mathcal{Q} = (4\pi)^{-1} \int \mathcal{J} dS$  is total topological charge of the skyrmion [62]. The expression (18) directly follows from (15) and (17), if the orthogonality property (12) of the eigenfunctions is applied. Definition of the skyrmion

center in form (18) was used in a number of papers [11, 49, 63–66].

Let us obtain the collective variable equations (14) in the approximation linear with respect to  $\xi_i$  and  $\dot{\xi}_i$ . For this purpose we substitute the Ansatz (15) into (14) and perform the integration using the orthogonality property (12) of the eigenfunctions. Finally one obtains the following components of the gyrotensor

$$G_{\mathcal{A}_\mu \mathcal{A}_{\mu'}} = G_{\mathcal{B}_\mu \mathcal{B}_{\mu'}} = 0, \quad G_{\mathcal{A}_\mu \mathcal{B}_{\mu'}} = -\frac{\alpha_\mu}{2} \delta_{\mu, \mu'}, \quad (19)$$

where  $\alpha_\mu = \int_0^\infty \rho f_\mu g_\mu d\rho$ . Note that  $\alpha_1 = 2Q$ . Effective energy, which corresponds to the model (15) has the form (up to the second order terms in  $\mathcal{A}_\mu$  and  $\mathcal{B}_\mu$ )

$$\mathcal{E} = \frac{1}{8} \sum_{\mu} \varepsilon_{\mu} (\mathcal{A}_{\mu}^2 + \mathcal{B}_{\mu}^2) + \mathcal{E}_0. \quad (20)$$

Here  $\varepsilon_{\mu} = \varepsilon_{\mu}^f + \varepsilon_{\mu}^g$ , see (A6), and  $\mathcal{E}_0$  is a part of energy which is independent on the collective variables. Expression (20) is a result of the straightforward integration of the energy (1), when the property (A8) is utilized.

Substituting (19) and (20) into (14) one obtains the set of equations for collective coordinates

$$\begin{aligned} \xi_i = \mathcal{A}_1 : \quad \dot{\mathcal{B}}_1 &= 0, \\ \xi_i = \mathcal{B}_1 : \quad \dot{\mathcal{A}}_1 &= 0, \\ \xi_i = \mathcal{A}_{\mu \neq 1} : \quad \dot{\mathcal{B}}_{\mu} &= -\omega_{\mu} \mathcal{A}_{\mu}, \\ \xi_i = \mathcal{B}_{\mu \neq 1} : \quad \dot{\mathcal{A}}_{\mu} &= \omega_{\mu} \mathcal{B}_{\mu}, \end{aligned} \quad (21)$$

where the properties (A5) and (A11) were utilized. Following the terminology of Ref. 29 one can conclude from (21) that the mode  $|1\rangle$  is a *special zero normal mode*, which in contrast to *inertial zero normal mode* [29] does not lead to mass generation. Introducing now a driving potential  $\mathcal{E} \rightarrow \mathcal{E} + \mathcal{U}(\mathcal{X}, \mathcal{Y})$ , which is assumed to be small enough in order not to change the eigenfunctions significantly, and taking into account (17), one obtains from (14) the well known Thiele equation for a massless particle [10, 55, 59]

$$\left[ \mathbf{e}_z \times \dot{\mathcal{R}} \right] - \partial_{\mathcal{R}} \mathcal{U} = 0. \quad (22)$$

Earlier it was shown [67] that in the absence of an external driving the translational mode of the magnetic vortex in an easy-plane ferromagnet does not exist. In other words, the zero translational mode is not inertial [29] for this case. The same results are valid for the case of magnetic skyrmion in a ferromagnetic film with the perpendicularly oriented easy-axis, when the analysis proposed in Ref. 67 is applied. Thus the inertial mass term is not expected in equations for collective coordinates for the case of a ferromagnetic vortex as well as for the ferromagnetic skyrmion. This is in contrast to the case of antiferromagnets [68] and weak ferromagnets [69], where the mass term appears in a natural

way, since the second order time derivative is initially present in the equation of motion written in terms of the Néel order parameter [70–73]. However, the inertial mass term is often used in collective coordinates equations for ferromagnetic vortices [10, 33–36], precessional solitons [37–39, 74] and skyrmions [8, 28, 40]. In part, this ambiguity originates from alternative methods of definitions of the soliton center. A frequently used method is based on the first moment of the perpendicular magnetization component [28, 29, 40, 49]

$$\mathbf{R} \equiv (X, Y) = \frac{\int \mathbf{r} (1 - m_z) d\mathcal{S}}{\int (1 - m_z) d\mathcal{S}}. \quad (23)$$

Thus  $\mathbf{R}$  signifies the “center of mass” of the  $m_z$  distribution. Using (15) one obtains (in a linear approximation in amplitudes  $\mathcal{A}_i, \mathcal{B}_i$ )

$$X = c_1 \mathcal{A}_1 + c_{-1} \mathcal{A}_{-1}, \quad Y = c_1 \mathcal{B}_1 - c_{-1} \mathcal{B}_{-1}, \quad (24)$$

where  $c_i = \frac{1}{2} \int_0^\infty \rho^3 g_1(\rho) f_i(\rho) d\rho / \int_0^\infty \rho (1 - \cos \Theta(\rho)) d\rho$ . In this way a formal coupling between modes  $|1\rangle$  and  $|-1\rangle$  is introduced into the system and, as a result, an effective mass term appears [28, 29]. Indeed, excluding amplitudes  $\mathcal{A}_{-1}$  and  $\mathcal{B}_{-1}$  from equations (14) and (24) one obtains a set of second order ODE for  $X$  and  $Y$ . For the case of a radially symmetrical potential  $\mathcal{U} = \omega_G \mathcal{R}^2 / 2$  they can be written in the vector form

$$\mathcal{M} \ddot{\mathbf{R}} - \left[ \mathbf{e}_z \times \dot{\mathbf{R}} \right] + k \mathbf{R} = 0, \quad (25)$$

where  $\mathcal{M} = 1/(\omega_{-1} - \omega_G)$  and  $k = \omega_{-1} \omega_G / (\omega_{-1} - \omega_G)$ . However, it should be emphasized that treatment of the position vector  $\mathbf{R} \neq \mathcal{R}$  as a skyrmion collective coordinate is not physically sound because  $\mathbf{R}$  does not describe the skyrmion displacement in the sense of the traveling wave model.

## VI. CONCLUSIONS

Main results of this paper are as follows: (i) we obtain asymptotic behavior of localized magnon modes over the chiral skyrmion, see (13); (ii) the high-frequency gyrotropic mode is always present in the spectrum, however its frequency practically coincides with the edge of the magnon continuum, except vicinity of the critical point  $|d| = 4/\pi$ ; (iii) using the orthogonality relation (12) for the magnon eigenfunctions we show that the collective skyrmion coordinates, which describe its motion in terms of the traveling-wave model, coincides with the first moment of the topological charge distribution; (iv) in terms of these collective coordinates the skyrmion dynamics is massless.

## VII. ACKNOWLEDGMENTS

V.P.K. and D.D.S. acknowledge the Alexander von Humboldt Foundation for the support. This work has been supported by the DFG via SFB 1143.

## Appendix A: Properties of the magnon spectrum

For each given value of  $\mu$  the EVP (11) generates a “ $\nu$ -spectrum”, which is described by the eigenfunctions  $f_{\mu,\nu}$  and  $g_{\mu,\nu}$  with the corresponding eigenfrequencies  $\omega_{\mu,\nu}$ . They are determined by the EVP

$$\mathcal{H}_\mu \psi_\mu = \omega_\mu \psi_\mu, \quad (\text{A1})$$

where  $\psi_\mu = (f_\mu, g_\mu)^\top$  and  $\mathcal{H}_\mu = \sigma_x H$ , see (11b). Operator  $\mathcal{H}_\mu$  is hermitian in a Hilbert space  $\mathbb{H}^\mu$  with scalar product

$$\langle \psi_{\mu,\nu} | \psi_{\mu,\nu'} \rangle \equiv \int_0^\infty \rho \psi_{\mu,\nu}^\top \sigma_x \psi_{\mu,\nu'} d\rho. \quad (\text{A2})$$

This results in real valued eigenfrequencies  $\omega_{\mu,\nu}$ , and (A2) enables us to formulate the orthogonality condition (for the given  $\mu$ ):

$$\int_0^\infty \rho [f_{\mu,\nu} g_{\mu,\nu'} + f_{\mu,\nu'} g_{\mu,\nu}] d\rho = C \delta_{\nu,\nu'} \quad (\text{A3})$$

with  $C$  being the normalization constant.

Assuming that for all  $\mu$  the EVP (A1) has no degenerate eigenvalues, one can present the general solution of (10) in form of partial wave expansion

$$\begin{aligned} \vartheta &= \sum_{\mu=-\infty}^{\infty} \sum_{\nu} f_{\mu,\nu}(\rho) [\bar{A}_{\mu,\nu} \cos(\mu\chi + \omega_{\mu,\nu}\tau) \\ &\quad - \bar{B}_{\mu,\nu} \sin(\mu\chi + \omega_{\mu,\nu}\tau)], \quad (\text{A4}) \\ \varphi &= \sum_{\mu=-\infty}^{\infty} \sum_{\nu} g_{\mu,\nu}(\rho) [\bar{A}_{\mu,\nu} \sin(\mu\chi + \omega_{\mu,\nu}\tau) \\ &\quad + \bar{B}_{\mu,\nu} \cos(\mu\chi + \omega_{\mu,\nu}\tau)]. \end{aligned}$$

Equations (A1) are invariant with respect to the simultaneous transformation  $\omega_\mu \rightarrow -\omega_{-\mu}$ ,  $f_\mu \rightarrow f_{-\mu}$ ,  $g_\mu \rightarrow -g_{-\mu}$ , and  $\mu \rightarrow -\mu$ . It means that the  $\nu$ -spectra can be split into the pairs  $\bar{\nu} = \{\nu', \nu''\}$ , which have the properties  $\omega_{\mu,\nu'} = -\omega_{-\mu,\nu''}$ ,  $f_{\mu,\nu'} = f_{-\mu,\nu''}$ , and  $g_{\mu,\nu'} = -g_{-\mu,\nu''}$ . This symmetry is schematically shown in the Fig. 4(a). It can be utilized in order to present the general solution in a form, which coincides with (A4) but: (i) summation over  $\nu$  is replaced by summation over pairs  $\bar{\nu} = \{\nu', \nu''\}$  and for each pair the only one index  $\nu \in \{\nu', \nu''\}$  is chosen, which corresponds to a *certain sign of the frequency*  $\omega_{\mu,\nu}$ ; (ii)  $\bar{A}_{\mu,\nu} \rightarrow A_{\mu\nu} = \bar{A}_{\mu,\nu'} + \bar{A}_{-\mu,\nu''}$  and  $\bar{B}_{\mu,\nu} \rightarrow B_{\mu\nu} = \bar{B}_{\mu,\nu'} - \bar{B}_{-\mu,\nu''}$ .

Analyzing numerically the spectrum of the EVP (A1) we found a number of localized modes with  $|\omega_{\mu,\nu}| < 1$ . Remarkably for each given  $\mu$  there is no more than one pair  $\bar{\nu} = \{\nu', \nu''\}$ , which corresponds to the localized modes, see Fig. 4(b). This fact and the above described possibility to fix the sign of the frequency, enables one to omit index  $\nu$  when classifying the localized modes. Thus,

in the following we consider that for each given  $\mu$  there is no more than one localized mode with eigenfunctions  $f_\mu(\rho)$ ,  $g_\mu(\rho)$ , and eigenfrequency  $\omega_\mu \geq 0$  (the equality takes place for  $\mu = 1$  only). Several examples of eigenfunctions are shown in the Fig. 3.

The eigenfunctions have a number of useful properties. First of all, for the case of the localized modes, the described above symmetry between branches  $\mu$  and  $-\mu$  enable one to write the orthogonality condition (A3) in form (12).

The next important property is integral relations between the eigenfrequencies and the eigenfunctions:

$$\omega_\mu = \frac{\varepsilon_\mu^f}{\alpha_\mu} = \frac{\varepsilon_\mu^g}{\alpha_\mu} = \frac{\kappa_\mu^f}{\beta_\mu} = \frac{\kappa_\mu^g}{\beta_\mu}. \quad (\text{A5})$$

Here the condition

$$\varepsilon_\mu^f = \varepsilon_\mu^g, \quad (\text{A6})$$

where

$$\varepsilon_\mu^f = \int_0^\infty \rho \left[ f_\mu'^2 + \left( \frac{\mu^2}{\rho^2} + U_1 \right) f_\mu^2 + \mu W f_\mu g_\mu \right] d\rho, \quad (\text{A7})$$

$$\varepsilon_\mu^g = \int_0^\infty \rho \left[ g_\mu'^2 + \left( \frac{\mu^2}{\rho^2} + U_2 \right) g_\mu^2 + \mu W f_\mu g_\mu \right] d\rho,$$

means that the energy is equally distributed between  $f$  and  $g$  components of the mode. And the condition

$$\kappa_\mu^f = \kappa_\mu^g, \quad (\text{A8})$$

where

$$\begin{aligned} \kappa_\mu^f &= \int_0^\infty \rho \left[ f_\mu' f_{-\mu}' + \left( \frac{\mu^2}{\rho^2} + U_1 \right) f_\mu f_{-\mu} + \mu W f_{-\mu} g_\mu \right] d\rho, \\ \kappa_\mu^g &= \int_0^\infty \rho \left[ g_\mu' g_{-\mu}' + \left( \frac{\mu^2}{\rho^2} + U_2 \right) g_\mu g_{-\mu} + \mu W f_\mu g_{-\mu} \right] d\rho, \end{aligned} \quad (\text{A9})$$

results in absence of coupling between modes  $|\mu\rangle$  and  $|-\mu\rangle$ . Here

$$\alpha_\mu = \int_0^\infty \rho f_\mu g_\mu d\rho, \quad \beta_\mu = \int_0^\infty \rho f_\mu g_{-\mu} d\rho. \quad (\text{A10})$$

Note that  $\beta_\mu = \beta_{-\mu}$ , while  $\alpha_\mu \neq \alpha_{-\mu}$ . For case of translational mode one has  $\alpha_1 = 2$  and also

$$\varepsilon_1^f = \varepsilon_1^g = \kappa_1^f = \kappa_1^g = 0, \quad (\text{A11})$$

which results in zero eigenfrequency  $\omega_1 = 0$ .

All properties (A5), (A6), (A8), (A11) directly follow from Eq. (11), which have the explicit form

$$-\Delta_\rho f_\mu + \left( \frac{\mu^2}{\rho^2} + U_1 \right) f_\mu + \mu W g_\mu = \omega_\mu g_\mu, \quad (\text{A12a})$$

$$-\Delta_\rho g_\mu + \left( \frac{\mu^2}{\rho^2} + U_2 \right) g_\mu + \mu W f_\mu = \omega_\mu f_\mu. \quad (\text{A12b})$$

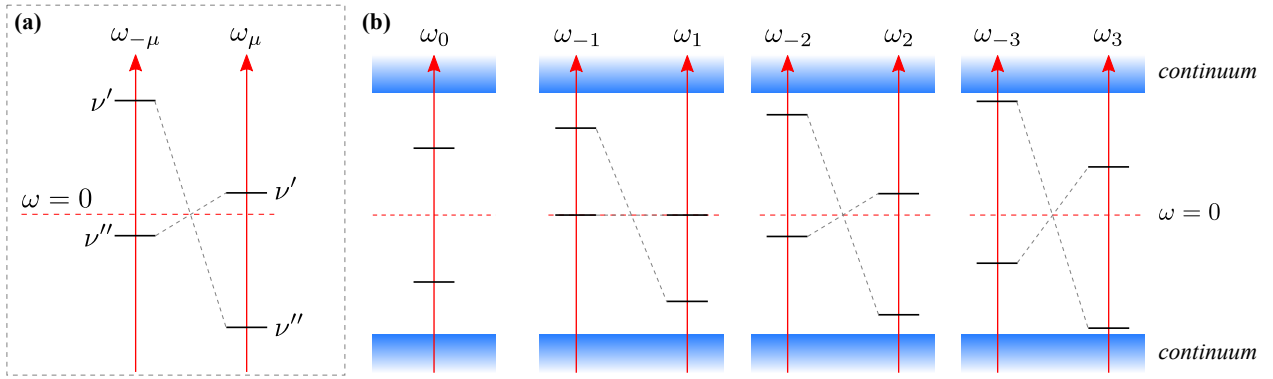


FIG. 4. Schematics of the magnon spectrum. Panel (a) demonstrates the symmetry between branches  $\mu$  and  $-\mu$  (only one pair  $\{\nu', \nu''\}$  is shown). Panel (b) shows the structure of the localized mode spectrum for  $|\mu| \leq 3$ .

Using the integration by parts one can present the quantity  $\varepsilon_\mu^f$  in the form

$$\varepsilon_\mu^f = \int_0^\infty \rho \left[ -\Delta_\rho f_\mu + \left( \frac{\mu^2}{\rho^2} + U_1 \right) f_\mu + \mu W g_\mu \right] f_\mu d\rho. \quad (\text{A13})$$

Applying now (A12a) one obtains  $\varepsilon_\mu^f = \omega_\mu \alpha_\mu$ . In the similar way, using (A12b) one obtains  $\varepsilon_\mu^g = \omega_\mu \alpha_\mu$ . The property (A8) can be proved analogously by applying the same procedure for the quantities  $\kappa_\mu^f$  and  $\kappa_\mu^g$ . The property (A11) can be checked straightforwardly by substituting into (A12) the explicit form of the eigenfunctions  $f_1 = -\Theta'$  and  $g_1 = \sin \Theta / \rho$ . All properties (12), (A6), (A8), (A5), (A11) have been verified numerically.

In order to estimate the asymptotic behavior of the eigenfrequencies for the case  $R_s \gg 1$  we apply the variational approach [37] with the following trial functions

$$f_\mu = \frac{a_\mu}{\cosh \frac{\rho - R_s}{|\delta|}}, \quad g_\mu = \frac{b_\mu}{\rho \cosh \frac{\rho - R_s}{|\delta|}}. \quad (\text{A14})$$

Substituting (A14) into (A6) one obtains

$$\begin{aligned} \varepsilon_\mu^f &\approx \frac{2}{R_s} (\mu^2 a_\mu^2 - \mu a_\mu b_\mu) + \mathcal{C}_\mu^f \frac{a_\mu^2}{R_s^3} + \mu \mathcal{C}_\mu^g \frac{a_\mu b_\mu}{R_s^3}, \\ \varepsilon_\mu^g &\approx \frac{2}{R_s} (b_\mu^2 - \mu a_\mu b_\mu) + \mathcal{C}_\mu^g \frac{b_\mu^2}{R_s^3} + \mu \mathcal{C}_\mu^f \frac{a_\mu b_\mu}{R_s^3}. \end{aligned} \quad (\text{A15})$$

Generally  $\mathcal{C}_\mu^f \neq \mathcal{C}_\mu^g$ . This means that for the used ansatz (A14) the conditions  $\varepsilon_\mu^f = \varepsilon_\mu^g$  and  $\varepsilon_1^f = \varepsilon_1^g = 0$  can be satisfied simultaneously only with accuracy  $\mathcal{O}(R_s^{-3})$ . In this case  $b_\mu = |\mu| a_\mu$ . Using now the expressions for eigenfrequencies (A5) and taking into account that  $\alpha_\mu \approx 2\delta a_\mu b_\mu$ , one obtains  $\omega_\mu \approx 2|\mu|R_s^{-1}$  when  $\mu < 0$  and  $\omega_\mu \approx c_\mu R_s^{-3}$

when  $\mu > 0$ . The constant  $c_\mu$  can not be determined in frames of the model (A14). Comparison with the numerical solution enables one to suppose that  $c_\mu = \mu(\mu^2 - 1)/2$ .

### Appendix B: Generalized Schrödinger equation

Introducing function  $\psi = \vartheta + i\varphi$  one can write (10) in form of so called generalized Schrödinger equation [38, 56],

$$-i\partial_\tau \psi = \mathcal{H}\psi + \mathcal{W}\psi^*, \quad \mathcal{H} = (-i\nabla - \mathbf{A})^2 + \mathcal{U} \quad (\text{B1})$$

with the potentials

$$\begin{aligned} \mathbf{A}(\rho) &= A e_\chi, \quad A = -\frac{\cos \Theta}{\rho} + \frac{|d|}{2} \sin \Theta, \\ \mathcal{U}(\rho) &= \frac{U_1 + U_2}{2} - A^2, \\ \mathcal{W}(\rho) &= \frac{U_1 - U_2}{2}. \end{aligned} \quad (\text{B2})$$

The vector function  $\mathbf{A}$  acts as a vector potential of effective magnetic field with the flux density

$$\mathbf{B} = \nabla \times \mathbf{A} = B \hat{z}, \quad B = \frac{\left( -\cos \Theta + \frac{|d|}{2} \rho \sin \Theta \right)'}{\rho}. \quad (\text{B3})$$

The first term in (B3) is the gyrocoupling density: finally the total flux is determined by  $\pi_2$  topology of the skyrmion, cf. Ref. 56

$$\Phi = \int B d^2x = -4\pi\Omega. \quad (\text{B4})$$

\* vkravchuk@bitp.kiev.ua

[1] J Ping Liu, Zhidong Zhang, and Guoping Zhao, *Skyrmions: Topological Structures, Properties, and Ap-*



- plications (Series in Materials Science and Engineering)* (CRC Press, Taylor & Francis Group, Boca Raton, FL, 2016).
- [2] Jan Seidel, ed., *Topological Structures in Ferroic Materials* (Springer International Publishing, 2016).
  - [3] Roland Wiesendanger, “Nanoscale magnetic skyrmions in metallic films and multilayers: a new twist for spintronics,” *Nature Reviews Materials* **1**, 16044 (2016).
  - [4] Naoto Nagaosa and Yoshinori Tokura, “Topological properties and dynamics of magnetic skyrmions,” *Nature Nanotechnology* **8**, 899–911 (2013).
  - [5] A. N. Bogdanov and D. A. Yablonskiĭ, “Thermodynamically stable “vortices” in magnetically ordered crystals. the mixed state of magnets,” *Zh. Eksp. Teor. Fiz.* **95**, 178–182 (1989).
  - [6] A. Bogdanov and A. Hubert, “Thermodynamically stable magnetic vortex states in magnetic crystals,” *Journal of Magnetism and Magnetic Materials* **138**, 255–269 (1994).
  - [7] A. Bogdanov and U. Rößler, “Chiral symmetry breaking in magnetic thin films and multilayers,” *Physical Review Letters* **87**, 037203 (2001).
  - [8] B. A. Ivanov, V. A. Stephanovich, and A. A. Zhmudskii, “Magnetic vortices — The microscopic analogs of magnetic bubbles,” *J. Magn. Magn. Mater.* **88**, 116–120 (1990).
  - [9] E. Kamenetskii, ed., *Electromagnetic, magnetostatic, and exchange-interaction vortices in confined magnetic structures* (Research Signpost, Kerala, India, 2008).
  - [10] F. G. Mertens and A. R. Bishop, “Dynamics of vortices in two-dimensional magnets,” in *Nonlinear Science at the Dawn of the 21st Century*, edited by P. L. Christiansen, M. P. Soerensen, and A. C. Scott (Springer-Verlag, Berlin, 2000) pp. 137–170.
  - [11] N. Papanicolaou and T. N. Tomaras, “Dynamics of magnetic vortices,” *Nuclear Physics B* **360**, 425–462 (1991).
  - [12] Albert Fert, Vincent Cros, and Joao Sampaio, “Skyrmions on the track,” *Nature Nanotechnology* **8**, 152–156 (2013).
  - [13] J. Sampaio, V. Cros, S. Rohart, A. Thiaville, and A. Fert, “Nucleation, stability and current-induced motion of isolated magnetic skyrmions in nanostructures,” *Nature Nanotechnology* **8**, 839–844 (2013).
  - [14] Xichao Zhang, G. P. Zhao, Hans Fangohr, J. Ping Liu, W. X. Xia, J. Xia, and F. J. Morvan, “Skyrmion-skyrmion and skyrmion-edge repulsions in skyrmion-based racetrack memory,” *Scientific Reports* **5**, 7643 (2015).
  - [15] Stefan Krause and Roland Wiesendanger, “Spintronics: Skyrmionics gets hot,” *Nature Materials* **15**, 493–494 (2016).
  - [16] Wang Kang, Yangqi Huang, Chentian Zheng, Weifeng Lv, Na Lei, Youguang Zhang, Xichao Zhang, Yan Zhou, and Weisheng Zhao, “Voltage controlled magnetic skyrmion motion for racetrack memory,” *Scientific Reports* **6**, 23164 (2016).
  - [17] A. V. Chumak, V. I. Vasyuchka, A. A. Serga, and B. Hillebrands, “Magnon spintronics,” *Nat Phys* **11**, 453–461 (2015).
  - [18] Andrii V. Chumak, Alexander A. Serga, and Burkard Hillebrands, “Magnon transistor for all-magnon data processing,” *Nature Communications* **5**, 4700 (2014).
  - [19] T. Schneider, A. A. Serga, B. Leven, B. Hillebrands, R. L. Stamps, and M. P. Kostylev, “Realization of spin-wave logic gates,” *Appl. Phys. Lett.* **92**, 022505 (2008).
  - [20] O. Klein, G. de Loubens, V. V. Naletov, F. Boust, T. Guillet, H. Hurdequint, A. Leksikov, A. N. Slavin, V. S. Tiberkevich, and N. Vukadinovic, “Ferromagnetic resonance force spectroscopy of individual submicron-size samples,” *Phys. Rev. B* **78**, 144410 (2008).
  - [21] V. Castel, J. Ben Youssef, F. Boust, R. Weil, B. Pigeau, G. de Loubens, V. V. Naletov, O. Klein, and N. Vukadinovic, “Perpendicular ferromagnetic resonance in soft cylindrical elements: Vortex and saturated states,” *Phys. Rev. B* **85**, 184419 (2012).
  - [22] V. Novosad, F. Y. Fradin, P. E. Roy, K. S. Buchanan, K. Yu. Guslienko, and S. D. Bader, “Magnetic vortex resonance in patterned ferromagnetic dots,” *Phys. Rev. B* **72**, 024455 (2005).
  - [23] Christoph Schütte and Markus Garst, “Magnon-skyrmion scattering in chiral magnets,” *Phys. Rev. B* **90**, 094423 (2014).
  - [24] Shi-Zeng Lin, Cristian D. Batista, and Avadh Saxena, “Internal modes of a skyrmion in the ferromagnetic state of chiral magnets,” *Phys. Rev. B* **89**, 024415 (2014).
  - [25] Junichi Iwasaki, Aron J. Beekman, and Naoto Nagaosa, “Theory of magnon-skyrmion scattering in chiral magnets,” *Phys. Rev. B* **89**, 064412 (2014).
  - [26] Sarah Schroeter and Markus Garst, “Scattering of high-energy magnons off a magnetic skyrmion,” *Low Temp. Phys.* **41**, 1043–1053 (2015).
  - [27] Markus Garst, Johannes Waizner, and Dirk Grundler, “Collective spin excitations of helices and magnetic skyrmions: review and perspectives of magnonics in non-centrosymmetric magnets,” *Journal of Physics D: Applied Physics* **50**, 293002 (2017).
  - [28] Imam Makhfudz, Benjamin Krüger, and Oleg Tchernyshov, “Inertia and chiral edge modes of a skyrmion magnetic bubble,” *Phys. Rev. Lett.* **109**, 217201 (2012).
  - [29] F. J. Buijnsters, A. Fasolino, and M. I. Katsnelson, “Zero modes in magnetic systems: General theory and an efficient computational scheme,” *Physical Review B* **89**, 174433 (2014).
  - [30] Vanessa Li Zhang, Chen Guang Hou, Kai Di, Hock Siah Lim, Ser Choon Ng, Shawn David Pollard, Hyunsoo Yang, and Meng Hau Kuok, “Eigenmodes of nel skyrmions in ultrathin magnetic films,” *AIP Advances* **7**, 055212 (2017), <http://dx.doi.org/10.1063/1.4983806>.
  - [31] M. Mruczkiewicz, M. Krawczyk, and K. Y. Guslienko, “Spin excitation spectrum in a magnetic nanodot with continuous transitions between the vortex, bloch-type skyrmion, and néel-type skyrmion states,” *Physical Review B* **95**, 094414 (2017).
  - [32] Konstantin Y. Guslienko and Zuhra V. Gareeva, “Gyrotropic skyrmion modes in ultrathin magnetic circular dots,” *IEEE Magnetics Letters* **8**, 1–5 (2017).
  - [33] A. R. Völkel, G. M. Wysin, F. G. Mertens, A. R. Bishop, and H. J. Schnitzer, “Collective-variable approach to the dynamics of nonlinear magnetic excitations with application to vortices,” *Phys. Rev. B* **50**, 12711–12720 (1994).
  - [34] F. G. Mertens, H. J. Schnitzer, and A. R. Bishop, “Hierarchy of equations of motion for nonlinear coherent excitations applied to magnetic vortices,” *Phys. Rev. B* **56**, 2510 (1997).
  - [35] G. M. Wysin, “Magnetic vortex mass in two-dimensional easy-plane magnets,” *Phys. Rev. B* **54**, 15156–15162 (1996).

- [36] B. A. Ivanov, H. J. Schnitzer, F. G. Mertens, and G. M. Wysin, “Magnon modes and magnon-vortex scattering in two-dimensional easy-plane ferromagnets,” *Phys. Rev. B* **58**, 8464–8474 (1998).
- [37] D. D. Sheka, B. A. Ivanov, and F. G. Mertens, “Internal modes and magnon scattering on topological solitons in two-dimensional easy-axis ferromagnets,” *Phys. Rev. B* **64**, 024432 (2001).
- [38] B. A. Ivanov and D. D. Sheka, “Local magnon modes and the dynamics of a small-radius two-dimensional magnetic soliton in an easy-axis ferromagnet,” *JETP Lett.* **82**, 436–440 (2005).
- [39] D. D. Sheka, C. Schuster, B. A. Ivanov, and F. G. Mertens, “Dynamics of topological solitons in two-dimensional ferromagnets,” *The European Physical Journal B - Condensed Matter* **50**, 393–402 (2006).
- [40] Felix Büttner, C. Moutafis, M. Schneider, B. Krüger, C. M. Günther, J. Geilhufe, C. v. Korff Schmising, J. Mohanty, B. Pfau, S. Schaffert, A. Bisig, M. Foerster, T. Schulz, C. A. F. Vaz, J. H. Franken, H. J. M. Swagten, M. Kläui, and S. Eisebitt, “Dynamics and inertia of skyrmionic spin structures,” *Nat Phys* **11**, 225–228 (2015).
- [41] S. Rohart and A. Thiaville, “Skyrmion confinement in ultrathin film nanostructures in the presence of Dzyaloshinskii-Moriya interaction,” *Physical Review B* **88**, 184422 (2013).
- [42] A. Crépieux and C. Lacroix, “Dzyaloshinsky–Moriya interactions induced by symmetry breaking at a surface,” *Journal of Magnetism and Magnetic Materials* **182**, 341–349 (1998).
- [43] André Thiaville, Stanislas Rohart, Émilie Jué, Vincent Cros, and Albert Fert, “Dynamics of Dzyaloshinskii domain walls in ultrathin magnetic films,” *EPL (Europhysics Letters)* **100**, 57002 (2012).
- [44] Hongxin Yang, André Thiaville, Stanislas Rohart, Albert Fert, and Mairbek Chshiev, “Anatomy of Dzyaloshinskii-Moriya interaction at Co/Pt interfaces,” *Phys. Rev. Lett.* **115**, 267210 (2015).
- [45] I. E. Dzialoshinskii, “Thermodynamic theory of “weak” ferromagnetism in antiferromagnetic substances,” *Sov. Phys. JETP* **5**, 1259–1272 (1957).
- [46] I. E. Dzyaloshinskii, “Theory of helicoidal structures in antiferromagnets. i. nonmetals,” *Sov. Phys. JETP* **19**, 964–971 (1964).
- [47] A. A. Belavin and A. M. Polyakov, “Metastable states of a 2D isotropic ferromagnet,” *JETP Lett.* **22**, 245 (1975).
- [48] I. E. Dzyaloshinskii, “The theory of helicoidal structures in antiferromagnets. ii. metals,” *Sov. Phys. JETP* **20**, 223– (1965).
- [49] Stavros Komineas and Nikos Papanicolaou, “Skyrmion dynamics in chiral ferromagnets,” *Phys. Rev. B* **92**, 064412 (2015).
- [50] A O Leonov, T L Monchesky, N Romming, A Kubetzka, A N Bogdanov, and R Wiesendanger, “The properties of isolated chiral skyrmions in thin magnetic films,” *New J. Phys.* **18**, 065003 (2016).
- [51] D. J. Clarke, O. A. Tretiakov, G.-W. Chern, Ya. B. Bazaliy, and O. Tchernyshyov, “Dynamics of a vortex domain wall in a magnetic nanostrip: Application of the collective-coordinate approach,” *Phys. Rev. B* **78**, 134412 (2008).
- [52] B. Hillebrands and A. Thiaville, eds., *Spin dynamics in confined magnetic structures III*, Topics in Applied Physics, Vol. 101 (Springer, Berlin, 2006).
- [53] N. L. Schryer and L. R. Walker, “The motion of  $180^\circ$  domain walls in uniform dc magnetic fields,” *Journal of Applied Physics* **45**, 5406–5421 (1974).
- [54] A. Thiaville, J.M. Garcia, and J. Miltat, “Domain wall dynamics in nanowires,” *Journal of Magnetism and Magnetic Materials* **242–245**, 1061–1063 (2002).
- [55] A. P. Malozemoff and J. C. Slonzewski, *Magnetic domain walls in bubble materials* (Academic Press, New York, 1979).
- [56] Denis D. Sheka, Ivan A. Yastremsky, Boris A. Ivanov, Gary M. Wysin, and Franz G. Mertens, “Amplitudes for magnon scattering by vortices in two-dimensional weakly easy-plane ferromagnets,” *Phys. Rev. B* **69**, 054429 (2004).
- [57] It can be verified by direct substitution into (11).
- [58] R. Rajaraman, *Solitons and Instanton* (North-Holland, Amsterdam, 1982).
- [59] A. A. Thiele, “Steady-state motion of magnetic of magnetic domains,” *Phys. Rev. Lett.* **30**, 230–233 (1973).
- [60] A. A. Thiele, “Applications of the gyrocoupling vector and dissipation dyadic in the dynamics of magnetic domains,” *J. Appl. Phys.* **45**, 377–393 (1974).
- [61] A. Hubert and R. Schäfer, *Magnetic domains: the analysis of magnetic microstructures* (Springer-Verlag, Berlin, 1998).
- [62] For the considered boundary conditions (3) one has  $\Omega = 1$ .
- [63] N. Papanicolaou and W. J. Zakrzewski, “Dynamics of interacting magnetic vortices in a model Landau–Lifshitz equation,” *Physica D: Nonlinear Phenomena* **80**, 225–245 (1995).
- [64] N. Papanicolaou and W. J. Zakrzewski, “Dynamics of magnetic bubbles in a Skyrme model,” *Physics Letters A* **210**, 328–336 (1996).
- [65] S. Komineas and N. Papanicolaou, “Topology and dynamics in ferromagnetic media,” *Physica D: Nonlinear Phenomena* **99**, 81–107 (1996).
- [66] N. Papanicolaou and P. N. Spathis, “Semitopological solitons in planar ferromagnets,” *Nonlinearity* **12**, 285–302 (1999).
- [67] A. V. Nikiforov and É. B. Sonin, “Dynamics of magnetic vortices in a planar ferromagnet,” *Soviet Physics - JETP* **58**, 373–378 (1983).
- [68] H Velkov, O Gomonay, M Beens, G Schwiete, A Brataas, J Sinova, and R A Duine, “Phenomenology of current-induced skyrmion motion in antiferromagnets,” *New Journal of Physics* **18**, 075016 (2016).
- [69] A. K. Zvezdin and K. A. Zvezdin, “Magnus force and the inertial properties of magnetic vortices in weak ferromagnets,” *Low Temperature Physics* **36**, 826–830 (2010).
- [70] I. V. Bar’yakhtar and B. A. Ivanov, “Nonlinear magnetization waves in the antiferromagnet,” *Sov. J. Low Temp. Phys.* **5**, 361 (1979).
- [71] A. F. Andreev and V. I. Marchenko, “Symmetry and macroscopical dynamics of a magnet,” *Sov. Phys. Usp.* **23**, 21 (1980).
- [72] Kjetil M. D. Hals, Yaroslav Tserkovnyak, and Arne Brataas, “Phenomenology of current-induced dynamics in antiferromagnets,” *Phys. Rev. Lett.* **106**, 107206

- (2011).
- [73] E. V. Gomonay and V. M. Loktev, “Spintronics of antiferromagnetic systems (review article),” *Low Temp. Phys.* **40**, 17–35 (2014).
- [74] B. A. Ivanov and V. A. Stephanovich, “Two-dimensional soliton dynamics in ferromagnets,” *Physics Letters A* **141**, 89–94 (1989).